Controlled Multi-Batch Self-Assembly of Micro Devices

Xiaorong Xiong[a], *Yael Hanein*[a], *Jiandong Fang*[a], *Yanbing Wang*[a],
Weihua Wang[b], *Daniel T. Schwartz*[b] *and Karl F. Böhringer*[a]
{xrxiong,hanein,karl}@ee.washington.edu
Dept of EE[a], *Dept of ChemE*[b], *University of Washington*
Seattle WA, 98195-2500

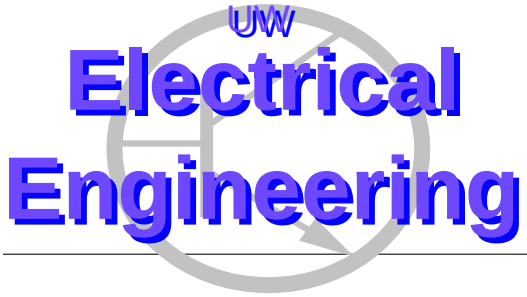

UWEE Technical Report
Number UWEETR-2002-0006
March 2002

Department of Electrical Engineering
University of Washington
Box 352500
Seattle, Washington 98195-2500
PHN: (206) 543-2150
FAX: (206) 543-3842
URL: http://www.ee.washington.edu

Controlled Multi-Batch Self-Assembly of Micro Devices

Xiaorong Xiong[a], Yael Hanein[a], Jiandong Fang[a], Yanbing Wang[a],
Weihua Wang[b], Daniel T. Schwartz[b] and Karl F. Böhringer[a]
{xrxiong,hanein,karl}@ee.washington.edu
Dept of EE[a], Dept of ChemE[b], University of Washington
Seattle WA, 98195-2500

University of Washington, Dept. of EE, UWEETR-2002-0006
March 2002

Abstract

A technique is described for assembly of multiple batches of micro components onto a single substrate. The substrate is prepared with hydrophobic alkanethiol-coated gold binding sites. To perform assembly, a hydrocarbon oil is applied to the substrate and wets exclusively the hydrophobic binding sites in water. Micro components are then added to the water, and assembled on the oil-wetted binding sites. Moreover, assembly can be controlled to take place on desired binding sites by using an electrochemical method to de-activate specific substrate binding sites. By repeatedly applying this technique, different batches of micro components can be assembled to a single substrate sequentially. As a post assembly procedure, electroplating is incorporated into the technique to establish electrical connections for assembled components. Important issues presented are: substrate fabrication techniques, electrochemical modulation by using suitable alkanethiol (dodecanethiol), electroplating of tin and lead alloy and binding site design simulations. Finally, we demonstrate a two-batch assembly of silicon square parts, and electrical connectivity by electroplating contacts to surface-mount light emitting diodes.

Keywords: micro assembly, self-assembly, hydrophobicity, capillary force, surface tension, interfacial energy, self-assembled monolayer, reductive desorption, electrochemical modulation, electroplating

1 Introduction

In the past two decades, major developments in micro electro mechanical systems (MEMS) have been founded on exploiting micromachining techniques and tools traditionally used for the silicon integrated circuits (ICs) industry. Current research in MEMS explores beyond what the name claims, and innovative materials and fabrication techniques have been combined with traditional semiconductor processes to build a wide range of micro functional devices (sensing, actuating, computing etc.). Integrated micro systems consisting of these functional components will find promising applications in areas such as telecommunications, chemical analysis and biomedical instrumentation. One major challenge in accomplishing such complex micro systems is the integration of different micro components. Monolithic integration of such systems is often limited by poor compatibility between components' fabrication processes or materials. Micro assembly provides a solution to circumvent these difficulties, and it allows micro devices to be fabricated and tested independently before they are integrated. Recently a number of techniques have been developed to assemble micro components into complex systems. A thorough study and analysis of various state of the art micro assembly strategies were presented by Cohn [1]. Conventional "pick and place" serial assembly methods have been adopted in the micro domain by using miniaturized robots and tools for organizing parts. There are two major concerns about this technique: serial manipulation and the "sticking problem". When a large number of parts need to be assembled, the time for assembly will be limited by the number of manipulators. In addition, with parts smaller than a millimeter, the adhesive forces between manipulator surfaces and parts, primarily due to electrostatic, van der Waals or surface tension, are significant compared to gravitational force [2]. Special manipulators and additional tools are required to overcome these difficulties [3–6].

In order to accomplish efficient micro assembly of a very large number of components, parallel assembly approaches have emerged, falling into two major categories: deterministic and stochastic. In the deterministic class,

assembly can be achieved by transferring microstructures between aligned wafers [7, 8]. In the stochastic category, assembly of a large number of identical micro parts occurs on specifically designed identical target sites. The assembly for all the micro components takes place simultaneously and the final assignment of each part to its destined site is random. Owing to the property that the assembly takes place spontaneously without external controls, the stochastic assembly is also referred to as "self-assembly", an adopted chemical term originally used to describe the process by which "programmed" molecular subunits spontaneously form complex supramolecular frameworks [9, 10]. Various driving forces have been employed for self-assembly. Yeh and Smith developed a process to assemble trapezoidal micro components into complementary holes in a substrate using fluidic flow and gravitation [11]. Böhringer et al. have proposed a micro assembly approach by employing electrostatic fields as the driving force, with the aid of ultrasonic vibration to overcome and eliminate friction and adhesion [12]. Surface tension, capable of driving different micro scale motions for various applications: high-resolution wet printing [13, 14]; a liquid-metal micromotor [15]; three-dimensional hinged micro structures [16], can also be involved as the driving force for micro assembly. Whitesides and coworkers first developed a strategy driven by capillary force to assemble simple electrical circuits [17, 18], and later three-dimensional electronic networks [19]. Srinivasan et al. adopted the capillary force driven assembly technique in [17, 18] to assemble microscopic parts onto desired sites on silicon and quartz substrates [20, 21]. In the studies in [17–21] parallel assembly was performed with identical components in a single batch step.

In this paper, we discuss a new approach to assemble multiple batches of components. In our approach, assembly is driven by capillary force and it proceeds on specially treated hydrophobic sites on the substrate as described in [20,21]. In addition, electrochemical modulation of the hydrophobicity of specific binding sites is used to alter the driving force for assembly. With this added innovation, assembly can be controlled to take place only on desired binding sites. By repeating the process to activate different sites on the substrate for assembly, different batches of micro parts can be assembled on a single substrate in a sequential manner. Electroplating is exploited as a post assembly process to establish electrical connections for assembled components, such as light emitting diodes (LEDs).

In the following sections, we discuss important issues of the technique: principle concepts of our two-batch micro assembly process, experimental details of the processes, and a simulation tool to evaluate and choose assembly binding site design for the substrate.

2 Process concept

In Figs. 1a-g, we illustrate the schematic flow of our self-assembly approach, which is explained step by step in this section. First, a supporting structure destined for the assembly (referred to as "substrate" hereafter) is fabricated with exposed clean hydrophilic gold (Au) patterns (Fig. 1a). The assembly "parts", defined as those objects that are to be assembled, are prepared with corresponding patterns. For simplicity, we use the term "binding sites" as the exposed gold patterns on the substrate and the corresponding patterns on the parts.

Second, the substrate is soaked in ethanolic alkanethiol ($CH_3(CH_2)_nSH$) solution and a hydrophobic alkanethiolate self-assembled monolayer (SAM) is chemisorbed on the exposed Au patterns [22]. The SAM adsorption activates all the Au binding sites on the substrate for assembly. The remaining areas on the substrate stay hydrophilic (Fig. 1b). In order to control the assembly to take place on selected binding sites, we use an electrochemical method to modulate the hydrophobicity of the binding sites we wish to de-active. Electrochemical desorption of alkanethiolate SAM from these binding sites [23, 24], i.e. $CH_3(CH_2)_nSAu + e^- \rightarrow Au + CH_3(CH_2)_nS^-$ changes them from hydrophobic to hydrophilic (Fig. 1c). Based on reductive desorption characterization of different alkanethiolate SAMs, discussed later in the text, we chose dodecanethiol ($CH_3(CH_2)_{11}SH$) for our assembly experiments. After the desorption process, assembly occurs only at the hydrophobic binding sites.

For assembly, the capillary driving force is created by a hydrocarbon-based lubricant liquid bridge between binding sites on a part and on a substrate in an aqueous environment. The lubricant is spread on a dry substrate. Since the interfacial tension of the lubricant-SAM interface ($\gamma < 1mJ/m^2$ [25]) is much lower than the interfacial tension of the water-SAM interface ($\gamma \approx 50mJ/m^2$ [25]), after immersion in water, the lubricant wets only the SAM-coated hydrophobic patterns. Parts are then transferred into water. As shown in Fig. 1d, capillarity aligns the part to a binding site on the substrate. This self-alignment phenomenon is the result of minimization of the interfacial energy between the lubricant bridges and water. Next, the lubricant is polymerized by heat and the parts are permanently bonded to the substrate. During the assembly process, the hydrophilic Au binding sites which have gone through SAM desorption remain clean and are reserved for future assembly. By repeating the SAM adsorption and assembly process, another batch of micro parts can be assembled on the vacant binding sites (Figs. 1e, f).

After assembly, different micro parts are physically bonded to the substrate. In most cases, electrical connections and controls for these parts are needed. An electroplating method has been investigated to fulfill these purposes. By electroplating, all the electrical connections between the assembled parts and the substrate can be established in a parallel manner (Fig. 1g).

We have so far discussed the principles of our technique. We now turn to describe the fabrication and experimental details for our multi-batch micro assembly process.

3 Experimental approaches

In this section we describe the principle experimental methods used to perform the self-assembly. This includes the fabrication process of suitable substrates and parts, SAM adsorption and selective desorption, assembly setup and finally electroplating process.

3.1 Fabrication of substrates and parts

3.1.1 Test part fabrication

For two-batch assembly, we use two types of 1×1mm silicon test parts. The first batch parts have square Au patterns (1×1mm) on one side, serving as the binding site, and Au patterns of 0.8×0.8mm on the other side. The second batch parts are patterned with 1×1mm Au binding sites on one side.

Commercial devices, i.e., LEDs (0.8×1.6mm, Lumex), are used as assembly components to demonstrate the electroplating method.

3.1.2 Substrate fabrication

In Figs. 2a-e, we show the schematic fabrication flow of a substrate designed to support self-assembly of square test parts. The substrate consists of two patterned layers on a silicon wafer. The substrate is prepared with a thermal oxidation layer of approximately 4500Å as an isolation layer on a 3" (100) silicon wafer (Fig. 2b). Next, the substrate is patterned with photoresist (AZ1512, Clariant), followed by a layer of 1100Å chrome(Cr)/gold(Au), sputtered on the substrate. The photoresist is then dissolved by acetone, and the metal layer is patterned on the substrate (Fig. 2c). The wafer is then cleaned with isopropanol alcohol (IPA), deionized (DI) water and dried with N_2. A passivation layer of spin-on glass (SOG) (311, Honeywell) is spun on, cured and photoresist AZ1512 is patterned as a mask to define the SOG pattern. This step is followed by a reactive ion etch (RIE, Trion technology) of CH_3F with O_2 to expose the Au binding sites. Finally, the substrate is cleaned with acetone to strip off the photoresist, rinsed with IPA, DI water and dried with N_2 (Figs. 2d,e).

Figs. 3a,b show the cross-section and a top view of a substrate designed for LED assembly and to demonstrate electroplating. To prepare such a substrate, a Cr/Au layer is patterned as binding sites for assembly. An additional metallization layer of 350Å Cr/nickel(Ni) is evaporated and patterned by lift-off, prior to the Cr/Au layer deposition. This additional Cr/Ni layer is patterned as electroplating metal bases for electroplating, as well as the connections between the Au binding sites and the electrical contacts (Fig. 3b). The electrical contacts serve as an interface to the external electrical control for the electroplating process, and to activate the LEDs afterwards. Silicon nitride is sputtered as a passivation layer. The passivation layer is then patterned photolithographically with a primer (prime-P10, Shin-EtsuMicroSi) and AZ1512 photoresist. The primer promotes photoresist adhesion. Finally, RIE of SF_6 is used to etch the silicon nitride layer to expose the binding sites and the electroplating bases. This step is followed by acetone, IPA, and DI water cleaning and N_2 dry.

3.2 Surface cleaning

Due to the nonpolar contaminants adsorbed on the high free energy Au surface [26], a cleaning process is crucial for our experiments. We use two minutes oxygen plasma process to clean the substrate.

3.3 SAM adsorption

Immediately after the oxygen plasma treatment, the cleaned substrate is placed into a glass container with freshly prepared alkanethiol solution. The solution is prepared with 1mM dodecanethiol ($(CH_3(CH_2)_{11}SH$, Aldrich) in ethanol, and the substrate is soaked in the solution for at least two hours to allow SAM adsorption. Thus, an alkanethiolate monolayer is deposited on exposed Au areas on the substrate. After the adsorption process, the exposed Au binding sites turn hydrophobic with a contact angle in the range of 110° [26].

3.4 Gold on mica samples

For the purpose of characterizing different alkanethiolate SAM desorption, we use single crystalline Au(111) thin film, evaporated on mica [27]. The samples are soaked in 1mM alkanethiol ($(CH_3(CH_2)_nSH$, n=2,7,11,17, Aldrich) solutions in ethanol for at least two hours to allow SAM adsorption.

3.5 SAM desorption

The electrochemical desorption of alkanethiolate SAMs is employed to modulate surface hydrophobicity. Reductive desorption of SAMs is performed in a conventional three-electrode electrochemical cell [28]. SAM coated Au surfaces, i.e. binding sites on fabricated wafers and Au(111) on mica samples, act as working electrodes. The counter electrode is a platinum mesh. A saturated calomel electrode (SCE, Accumet) is used as the reference electrode. The electrolyte is 0.5 M (pH=13.5) aqueous KOH (Fisher Scientific) solution. The potential is controlled between the working and reference electrodes, and the current which passes through the working electrode, electrolyte and counter electrode is measured. The control of the cell is performed by a potentiostat. Cyclic voltammetry (CV) (i.e., the repeated scanning of the working electrode potential) is performed to monitor and characterize the desorption of SAMs from working electrode surfaces [24]. The potential windows for the CVs are from $0V$ to $-1.4V$ vs. SCE. Lower pH solutions are not feasible, as the low desorption potentials of the SAMs (below $-1V$ vs SCE.) would have strong interference from the co-evolution of H_2.

3.6 Assembly and electroplating

After desorption of SAMs from the Au surfaces, the substrate is removed from the electrochemical bath, rinsed with DI water and dried with N_2. A hydrocarbon lubricant is spread on the clean, dry substrate by a pipette. To form lubricant droplets, the substrate is slid manually and slowly into DI water in a petri-dish until it is completely immersed in water. Parts are then cleaned with DI water and added into the petri-dish. The petri-dish is placed on an orbital shaker. With agitation, the assembly takes place exclusively on the hydrophobic areas with lubricant.

Here we use a heat-curable lubricant composed of 97wt.$\%$ triethyleneglycol dimethacrylate (Sigma) as a cross linker, and 3wt.$\%$ benzoyl peroxide (Sigma) as thermal initiator [29]. The lubricant, completely polymerized at 80°C in water after approximately an hour, permanently bonds the parts to the binding sites.

The plating process employs a platinum mesh as an anode and the plating bases on the substrate as a cathode. The bath is a commercial solder solution (Technic solder matte NF 820 HS (60/40), Technic Inc.). The plated solder is an alloy of lead (Pb) 40wt.$\%$ and tin (Sn) 60wt.$\%$. The current density for plating is 300mA/cm^2, and the plating rate is approximately 5μm/min. The resistivity of the alloy is approximately $1.4\times10^{-7}\Omega$m.

4 Binding site design

Binding site design is important for assembly, since optimal binding site design would allow high alignment accuracy, high assembly yield, short assembly time, or uniqueness of assembly orientation. When using commercial off the shelf components such as LEDs with given design shown in Fig. 4a, a straightforward design would simply use the same pattern as the part binding site shape. However, it was shown that such a design will not always be optimal and misalignment may occur in assembly [30]. To improve assembly, we custom design the binding site and plating basis geometry using a software simulation tool [30, 31].

The simulation tool is based on a simple surface energy model of our self-assembly system. It uses the observation that self-assembly and self-alignment is the result of minimization of interfacial energy between the lubricant meniscus and the aqueous environment. As described in [30, 31], the interfacial energy is directly proportional to the exposed

hydrophobic surfaces in water. In a first-order approximation, the surface energy W can be represented in terms of the hydrophobic regions on the part and the substrate, denoted by P and S respectively, as long as the lubricant bridge height is small compared to the binding site length or width:

$$W = \gamma(\mid S \mid + \mid P \mid -2 \mid S \cap P \mid) \tag{1}$$

Here γ is the interfacial energy coefficient, and $\mid S \mid$ and $\mid P \mid$ denote the surface area of a region S and P respectively. Since the terms $\mid S \mid$ and $\mid P \mid$ in Eq.1 are constants, W is directly proportional to $- \mid S \cap P \mid$: the negated overlap area between S and P. A concise and rigorous derivation of this model is presented in [31].

To briefly describe the implementation of the simulation tool, the overlap area called $A(x, y, \theta)$ is computed with respect to three parameters, representing the relative location (x, y) and orientation θ of P to S. For a given orientation θ, the value A can be calculated efficiently by two-dimensional convolution of P to S. To characterize the overlap area as a function of rotation angle, calculations are iterated for discretized θ values in the range from 0° to 360°. Therefore, for a binding site design, we use two plots to show the simulation results: translation and rotation. In the translation result, the overlap ratio, which is the ratio of the overlap area to part binding site area ($\frac{|S \cap P|}{|P|}$), is plotted as a function of relative location (x, y) of P to S. In the rotation result, each point in the plot corresponds to a maximum overlap ratio with respect to a given orientation θ.

Ideally, assembly configurations should possess a unique global energy minimum, which, according to our model, would correspond to a unique maximum of area overlap as a function of (x, y, θ). With the given symmetric LED binding site design shown in Fig. 4a, such a unique maximum is impossible to achieve. Figs. 4b, e show two different binding site designs, and the design in Fig. 4b is simply the same as the LED binding site design. Figs. 4c and d are the translation and rotation simulation results for design (b), and Figs. 4f and g are the simulation results for design (e). Fig. 4b shows multiple local maxima for binding site design (b) at 0°, while Fig. 4e shows only one maximum for design (e). Figs. 4c and f show that design (b) has multiple maxima at various orientations, while design (e) has only two maxima for 0° and 180° (there must be two maxima because the LED design is symmetric). These simulation results indicate that design (d) is preferable, as it exhibits only two maxima in overlap.

5 Results

We have described the experimental details of our approach to incorporate two additional methods, (1) selective desorption of SAM from patterned surfaces to allow multi-batch assembly, and (2) electroplating to establish electrical connectivity of assembled parts into the micro assembly tool box. To demonstrate these capabilities we fabricate and test substrates and parts specifically designed for these applications. Our results are presented below.

5.1 Selective desorption

Previous studies [22] show that monolayers formed by alkanethiols with longer chain lengths are more densely packed. This affects the stability of the monolayer. To find an optimal alkanethiol forming stable SAMs for assembly, but also possessing desorption time suitable for our application, we have explored reductive desorption of different alkanethiolate SAMs ($CH_3(CH_2)_nSH$, n=2,7,11,17). Cyclic voltammograms, obtained from single crystalline Au(111) on mica [23, 24], have been used for characterization.

Figs. 5a-c show results from the reductive desorption experiments of Au(111) on mica samples. The clear negative current peaks in the CVs indicate the reductive desorption of alkanethiolate SAMs from the surfaces. These peaks become less pronounced with additional CV scanning cycles, implying the decreasing coverage of SAMs. The disappearance of the desorption peaks indicates that a major portion of the SAM has been desorbed. The desorption peak shifts systematically with carbon chain length, with the $C_8H_{18}S$, $C_{12}H_{26}S$ and $C_{18}H_{38}S$ peaks being at $-1.05V$, $-1.2V$ and $-1.35V$ vs SCE (Figs. 5a-c). Also, the time needed to desorb the SAMs varies systematically with chain length. For example, the longest alkanethiolate SAM assessed, $C_{18}H_{38}S$, still has a significant fraction on the surface after one hour and half of desorption (Fig. 5c). On the other hand, we observe that the surface with propanethiolate SAM changes hydrophobicity in the KOH solution even in the absence of an applied potential. Therefore, propanethiol is ruled out as a choice for the assembly experiment. The longer desorption time for the longer chain length alkanethiolate SAMs might be the result of re-adsorption of the reduced products. The discussions in [32] suggest that the re-adsorption is attributed to the solubilities and diffusion rates of the alkanethiolate desorption products, with the longer alkanethiolates having the lower solubility and diffusion rate.

By comparing desorption time (Figs. 5a-c) and stability of the different alkanethiolate SAMs, dodecanethiol ($C_{12}H_{26}S$) is chosen for the assembly experiments. The dodecanethiol forms stable hydrophobic SAM on Au, and desorption of a major fraction of the monolayer takes approximately fifteen minutes implied by the disappearance of the desporption peak in the dotted CV data in Fig. 5b.

Desorption of dodecanethiolate SAM from polycrystalline Au patterns on a Si substrate is shown in Fig. 5d. These desorption CVs have broader peaks, compared with desorption CVs from single crystalline Au on mica. Moreover, it is observed that the time needed to desorb the SAM to turn Au surface hydrophilic is longer than the time measured by the disappearance of the desorption peak. The average desorption time for the designs shown in Fig. 2e is around one hour for dodecanethiolate SAM.

5.2 Two step assembly

A substrate shown in Fig. 2 is used to demonstrate two step assembly of square test parts. The substrate is first coated with dodecanethiolate SAM (Fig. 1b). Then selected sites undergo electrochemical desorption to return them to the hydrophilic state (Fig. 1c). After SAM adsorption and one hour selective desorption, the substrate with a thin layer of lubricant is immersed in water (Fig. 1d without part). The different lubricant wetting properties of Au binding sites with and without SAM are readily seen in Fig. 6a. The Au squares without SAM on the substrate remain lubricant free (Fig. 6a). Next, a first batch of parts are added to the aqueous phase and assembled on the lubricant coated layer (Fig. 6b). The square test parts are used as fabricated. Untreated Au surfaces have a contact angle of 70° [26] after exposure to lab atmosphere, which is sufficient to ensure assembly. After curing the lubricant and cleaning the substrate, a second assembly is performed by repeating steps described in Fig. 1e and f. An example of two-batch assembly is shown in Fig. 6c. By repeating SAM adsorption, desorption and assembly, controlled micro assembly is feasible, in principle, for a large number of batches.

5.3 Electroplating

We now turn to demonstrate the use of an electroplating method to establish electrical connections to assembled parts. Our choice of the electroplating basis metal is mainly based on the following considerations: compatibility with the substrate fabrication process and adhesion with electroplated alloy. Different metals: Au, aluminum (Al), titanium-tungsten (TiW) and Ni have been tested. The results are summarized in Table 1.

Metals	Process compatibility	Adhesion with alloy
Au	compatible.	good
Al	compatible.	poor
TiW	incompatible	poor
Ni	compatible.	good

Table 1. Comparisons between electroplating basis materials.

The poor adhesion on Al and TiW is due to their natural oxide layer, while Au does not have such a natural oxide layer. As a result, the plated alloy has uneven profile on Al and TiW plating bases. Good adhesion between Ni plating basis and the plated alloy is observed, despite the Ni oxide layer, which is thinner than the Al oxide [33]. The thin Ni oxide can be reduced at the plating potential in the acid electroplating solution, thus allowing good adhesion.

To demonstrate the electroplating method, we use LEDs for assembly by repeating the process described in Figs. 1a-d. The results are shown in Fig. 7. In Fig. 7a, we show a Au binding site with two Ni plating bases. The design is chosen based on the simulations results in Fig. 4. No alkanethiolate SAM is formed on the oxide coated Ni during the adsorption process. Thus during the assembly process, the lubricant does not wet the Ni plating bases, leaving them clean for electroplating (Fig. 7b). An assembled LED is aligned and bonded at the desired site after lubricant curing (Fig. 7c).

In Fig. 8a, we show an environmental scanning electron microscope (ESEM) image of an assembled LED. The gap between the LED and the substrate is approximately 20μm. Using the electroplating procedure described above, the gap is bridged by solder alloy (Fig. 8b) and assembled LEDs can be activated by applying voltage to the electrical contacts on the substrate (Fig. 3b). Measured contact resistance is 10Ω for the current design. An illustration of an activated glowing LED on a substrate is shown in Fig. 9.

5.4 Substrate material and durability

As discussed above, both Au and Ni are demonstrated as good electroplating basis metals. However, there are several considerations that make Ni advantageous. When using Au bases, an extra desorption process is needed to remove the alkanethiolate monolayer deposited on the bases. Also, we have observed severe wrinkling and peeling of SOG on Au after approximately two hours of desorption in the alkaline bath. This is due to poor adhesion between SOG and Au, particularly in alkaline solution (i.e. 0.5M KOH) with potential bias applied to the Au areas. Tests of silicon nitride on Au during the desorption process have also shown wrinkling results. To overcome these problems Ni is chosen as an additional metal for electroplating basis. The Ni layer is also patterned as connections between the Au binding sites and the electrical contacts (Fig. 3b) to reduce the contact area between Au and the passivation layer. With Ni beneath the passivation layer, it is observed that there are no signs of wrinkling after more than two hours, when performing SAM desorption.

6 Discussions

In the previous sections, we have demonstrated the feasibility of two-batch self-assembly and electroplating procedures. To ensure the applicability of these techniques to practical systems, issues such as yield, part properties, lubricant properties, and scaling effects have to be considered. In this section, we discuss these issues.

6.1 Yield

In practice, assembly of a large number of parts is desired. The yield is largely determined by the assembly setup. In our current setup, micro part movement is initiated by an orbital shaker and is two-dimensional. This is a simple setup used to demonstrate process feasibility, not specifically designed for high yield assembly. For example, flipped parts usually are not assembled. To achieve better yield, a large excess components have to be supplied into the system, and a setup allowing agitation also in the perpendicular direction is preferable [21].

6.2 Micro part properties

Our multi-batch assembly approach can be applied to a range of different micro parts. These parts have to be compatible with all assembly processes, such as electrochemical desorption, lubricant curing and electroplating.

Furthermore, with assembled micro parts having hydrophobic patterns on the backside, the repeatability of the assembly process might be limited. In such a situation, the lubricant will wet the hydrophobic patterns on the assembled components, and parts from the next batch will be attracted to these patterns during the later assembly step. On the other hand, this could be useful, if three dimensional stacks of parts are desired.

6.3 Lubricant properties

It was noted that lubricant thickness on the binding sites affects the assembly alignment [34]. Preliminary results show qualitative agreement with the simulations in [34]. The lubricant thickness is determined by the lubricant application, as well as the lubricant properties including surface tension, viscosity etc. [14, 35]. We plan to perform a study on the influences of these parameters on assembly results.

6.4 Scaling

In our experiments, assembly parts are in the millimeter scale. In [25] parts are in the range of 150-400μm and in [19] parts are up to 5mm in size. Even though these self-assembly methods have been successful with part size ranging from hundreds of micrometers to several millimeters, it is anticipated that similar results can be obtained at much smaller dimensions [36]. Obviously, part size is an important parameter in the assembly. To determine the optimal working domain for this technique the upper and lower bound of part size will be studied.

7 Summary

To summarize, we have established a protocol based on capillary force and surface hydrophobicity modulation for multi-batch micro self-assembly. Presented are the principles, fabrication, assembly, electroplating processes and pattern design of this technique. By incorporating a SAM desorption process into the self-assembly approach, multiple batch assembly becomes feasible. A two-batch micro assembly has been successfully demonstrated. The electroplating method is compatible with the parallel assembly process, and achieves electrical connectivity for assembled components simultaneously. As an enabling technique, our assembly approach is applicable to generic parts such as surface mount LEDs. It is anticipated that our controlled multi-batch self-assembly of micro devices technique can be applicable to a wide range of micro or nano parts made of different materials, for the integration and packaging of complex heterogeneous systems.

8 Acknowledgments

We would like to thank Roger T. Howe and Uthara Srinivasan for inspiring discussions, and Michael B. Cohn for providing some microparts, and Shaoyi Jiang and Shengfu Chen for their help with the mica samples preparation. We thank the members of the University of Washington MEMS lab and the staff and users of the Washington Technology Center Microfabrication laboratory for their help and support.

This research is supported in part by NSF Career Award ECS9875367 to K. Böhringer and by donations from Agilent Technologies, Intel Corporation, Microsoft Research, Tanner Research Inc. and Technic Inc. D. Schwartz acknowledges partial support by an NSF Young Investigator Award CTS-9457097. Y. Hanein acknowledges partial support by NSF CISE Postdoctoral Research Associateship EIA0072744. X. Xiong acknowledges support from a Ford Fellowship.

References

[1] M. B. Cohn, *Assembly Techniques for Microelectromechanical Systems. Ph.D Thesis*, University of California at Berkeley, Department of Electrical Engineering and Computer Sciences, 1997.

[2] R. S. Fearing, "Survey of sticking effects for micro-parts," in *Proc. IEEE/RSJ Int. Conf. on Robotics and Intelligent Systems (IROS)*, Pittsburg, PA, 1995, pp. 212 –217.

[3] S. J. Ralis, B. Vikramaditya, and B. J. Nelson, "Micropositioning of a weakly calibrated microassembly system using coarse-to-fine visual servoing strategies," *IEEE Transactions on Electronics Packaging Manufacturing*, vol. 23, no. 2, pp. 123 –131, 2000.

[4] G. Yang, J. A. Gaines, and B. J. Nelson, "A flexible experimental workcell for efficient and reliable wafer-level 3D micro-assembly," in *Proc. IEEE International Conference on Robotics and Automation (ICRA)*, Seoul, South Korea, 2001, pp. 133 – 138.

[5] J. A. Thompson and R. S. Fearing, "Automating microassembly with ortho-tweezers and force sensing," in *Proc. IEEE/RSJ International Conference on Intelligent Robots and Systems (IROS)*, Maui, HI, 2001, pp. 1327 –1334.

[6] K. Saitou, D. A. Wang, and S. J. Wou, "Externally resonated linear microvibromotor for microassembly," *ASME/IEEE J. of Microelectromechanical Systems*, vol. 9, no. 3, pp. 336–346, 2000.

[7] M. B. Cohn, K. F. Böhringer, J. M. Noworolski, A. Singh, C. G. Keller, K. Y. Goldberg, and R. T. Howe, "Microassembly technologies for MEMS," in *Proc. SPIE Micromachining and Microfabrication*, Santa Clara, CA, 1998, pp. 2–16.

[8] A. S. Holmes and S. M. Saidam, "Sacrificial layer process with laser-driven release for batch assembly operations," *ASME/IEEE J. of Microelectromechanical Systems*, vol. 7, no. 4, pp. 416–422, 1998.

[9] L. J. Barbour, G. W. Orr, and J. L. Atwood, "An intermolecular $(H_2O)_{10}$ cluster in a solid-state supramolecular complex," *Nature*, vol. 393, pp. 671 – 673, 1998.

[10] J. M. Lehn, "Supramolecular chemistry," *Science*, vol. 260, no. 5115, pp. 1762–1763, 1993.

[11] H. J. Yeh and J. S. Smith, "Fluidic assembly for the integration of GaAs light-emitting diodes on Si substrates," *IEEE Photonics Technology Letters*, vol. 46, pp. 706–709, 1994.

[12] K. F. Böhringer, K. Y. Goldberg, M. B. Cohn, R. T. Howe, and A. P. Pisano, "Parallel microassembly using electrostatic force fields," in *IEEE International Conference on Robotics and Automation (ICRA)*, Leuven, Belgium, 1998, pp. 483 – 496.

[13] A. A. Darhuber, S. M. Troian, and S. Wagner, "Physical mechanisms governing pattern fidelity in microscale offset printing," *Journal of Applied Physics*, vol. 90, no. 7, pp. 3602–3609, 2001.

[14] A. A. Darhuber, S. M. Troian, J. M. Davis, S. M. Miller, and S. Wagner, "Selective dip-coating of chemically micropatterned surfaces," *Journal of Applied Physics*, vol. 88, no. 9, pp. 5119–5126, 2000.

[15] J. Lee and C. J. Kim, "Surface-tension-driven microactuation based on continuous electrowetting," *ASME/IEEE J. of Microelectromechanical Systems*, vol. 9, no. 2, pp. 171–180, 2000.

[16] K. F. Harsh, R. S. Irwin, and Y. C. Lee, "Solder self-assembly for MEMS," in *Proceedings of the 1998 International Instrumentation Symposium (ISA)*, Reno, NV, 1998, pp. 256–261.

[17] A. Terfort, N. Bowden, and G. M. Whitesides, "Three-dimensional self-assembly of millimetre-scale components," *Nature*, vol. 386, pp. 162–164, 1997.

[18] A. Terfort and G. M. Whitesides, "Self-assembly of an operating electrical circuit based on shape complementarity and the hydrophobic effect," *Advanced Materials*, vol. 10, no. 6, pp. 470–473, 1998.

[19] D. Gracias, J. Tien, T. L. Breen, C. Hsu, and G. M. Whitesides, "Forming electrical networks in three dimensions by self-assembly," *Science*, vol. 289, pp. 1170–1172, 2000.

[20] U. Srinivasan, R. T. Howe, and D. Liepmann, "Fluidic microassembly using patterned self-assembled monolayers and shape matching," in *Proc. 1999 Int. Conf. on Solid-State Sensors and Actuators (Transducers)*, Japan, 1999, pp. 1170–1173.

[21] U. Srinivasan, D. Liepmann, and R. T. Howe, "Microstructure to substrate self-assembly using capillary forces," *ASME/IEEE J. of Microelectromechanical Systems*, vol. 10, no. 1, pp. 17–24, 2001.

[22] M. D. Porter, T. B. Bright, D. L. Allara, and C. E. D. Chidsey, "Spontaneously organized molecular assemblies. 4. structural characterization of n-alkyl thiol monolayers on gold by optical ellipsometry, infrared spectroscopy, and electrochemistry," *Journal of American Chemical Society*, vol. 109, no. 12, pp. 3359–3568, 1987.

[23] N. L. Abbot, A. B. Gorman, and G. M. Whitesides, "Active control of wetting using applied electrical potentials and self-assembled monolayers," *Langmuir*, vol. 11, no. 1, pp. 16–18, 1995.

[24] M. M. Walczak, D. D. Popenoe, R. S. Deinhammer, B. D. Lamp, C. Chung, and M. D. Porter, "Reductive desorption of alkanethiolate monolayers at gold: A measure of surface coverage," *Langmuir*, vol. 7, no. 11, pp. 2687–2693, 1991.

[25] U. Srinivasan, *Fluidic Self-Assembly of Microfabricated Parts to Substrates Using Capillary Forces. Ph.D Thesis*, University of California at Berkeley, Department of Chemical Engineering, 2001.

[26] C. D. Bain, E. B. Troughton, Y. T. Tao, J. Evall, G. M. Whitesides, and R. G. Nuzzo, "Formation of monolayer films by the spontaneous assembly of organic thiols from solution onto gold," *J. Am. Chem. Soc.*, vol. 111, pp. 321–335, 1989.

[27] S. Chen, L. Li, C. L. Boozer, and S. Jiang, "Controlled chemical and structural properties of mixed self-assembled monolayers of alkanethiols on Au(111)," *Langmuir*, vol. 16, no. 24, pp. 9287–9293, 2000.

[28] A. J. Bard and L. R. Faulkner, *Electrochemical Methods: Fundamentals and Applications*, John Wiley & Sons, New York, first edition, 1980.

[29] J. A. Pojman, W. W. West, and J. Simmons, "Propagating fronts of polymerization in the physical chemistry laboratory," *Journal of Chemical Education*, vol. 74, no. 6, pp. 727–730, 1997.

[30] K. F. Böhringer, U. Srinivasan, and R. T. Howe, "Modeling of capillary forces and binding sites for fluidic self-assembly," in *Proc. of IEEE Workshop on Micro Electro Mechanical Systems (MEMS)*, Switzerland, 2001, pp. 369–374.

[31] X. Xiong, Y. Hanein, W. Wang, D. T. Schwartz, and K. F. Böhringer, "Multi-batch micro-selfassembly via controlled capillary forces," in *Proc. IEEE/RSJ International Conference on Intelligent Robots and Systems (IROS)*, Maui, HI, 2001, pp. 1335 – 1342.

[32] C. J. Zhong and M. D. Porter, "Fine structure in the voltammetric desorption curves of alkanethiolate monolayers chemisorbed at gold," *Journal of Electroanalytical Chemistry*, vol. 425, pp. 147–153, 1997.

[33] J. W. Dini, *Electrodeposition: The Materials Science Of Coatings And Substrates*, Noyes Publications, New Jersey, 1993.

[34] A. Greiner, J. Lienemann, J. G. Korvink, X. Xiong, Y. Hanein, and K. F. Böhringer, "Capillary forces in microfluidic self-assembly," in *Fifth International Conference on Modeling and Simulation of Microsystems (MSM'02)*, San Juan, Puerto Rico, USA, April 22-25, 2002.

[35] A. A. Darhuber, S. M. Troian, S. M. Miller, and S. Wagner, "Morphology of liquid microstructures on chemically patterned surfaces," *Journal of Applied Physics*, vol. 87, no. 11, pp. 7768–7775, 2000.

[36] W. S. N. Trimmer, "Microrobots and micromechanical systems," *Sensors and Actuators*, vol. 19, no. 3, pp. 267–287, 1989.

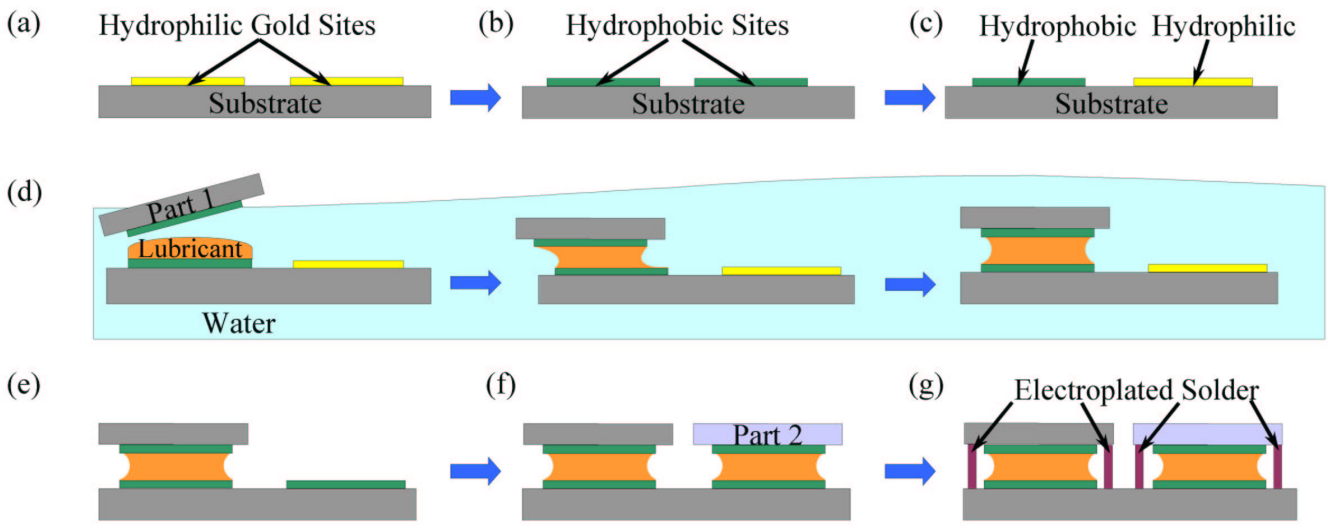

Figure 1: Schematics of two-batch assembly steps: (a) A fabricated substrate with electrically isolated regions of hydrophilic Au sites. (b) Alkanethiolate SAM adsorbed on Au patterns turns them hydrophobic. (c) Electrochemical SAM desorption from selected binding site (the right site) is used to de-activate it for assembly. (d) Application and partitioning of a hydrocarbon lubricant to hydrophobic binding site, followed by assembly of the part and lubricant curing in an aqueous environment. (e) Deposition of alkanethiolate SAM on the vacant Au binding site to activate it for another assembly. (f) Repeating the step in (d) for other micro parts. (g) Establishing electrical connections between assembled parts and the substrate by electroplating. Note that the vertical dimensions have been exaggerated for illustration purposes.

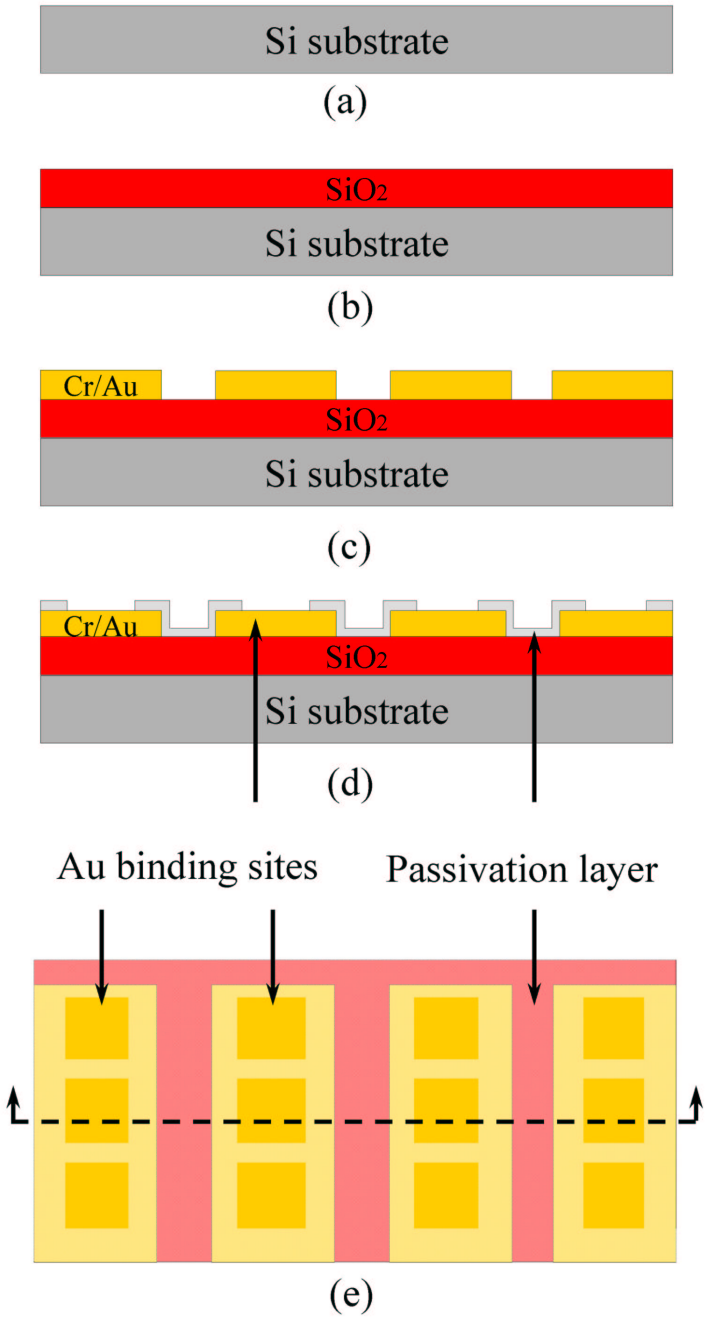

Figure 2: Fabrication flow of substrates designed for square test parts assembly. (a) Silicon substrate. (b) Silicon dioxide layer, which isolates the silicon substrate from the metal layer. (c) Cr/Au metallization layer. This layer is patterned as an array of electrically isolated Au stripes. (d) Passivation layer of SOG. This layer has openings that expose the square binding sites on the Au stripes. (e) Top view of a fabricated substrate.

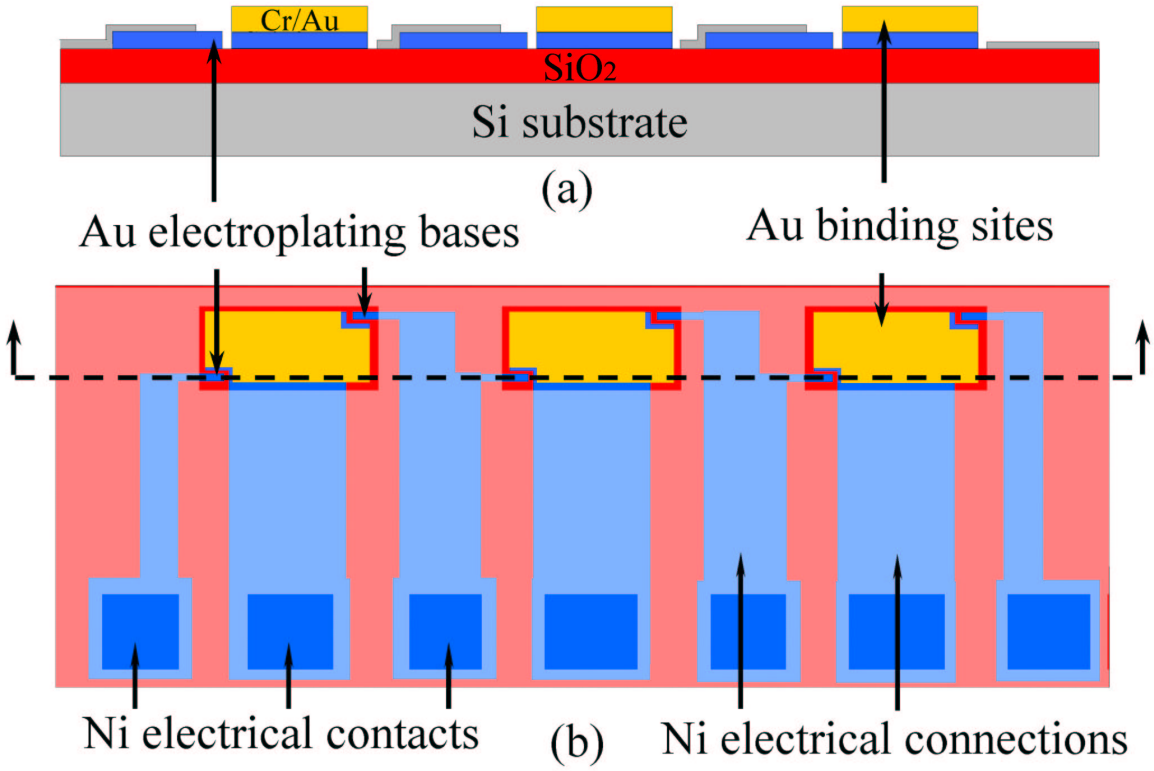

Figure 3: Schematic plots of a fabricated substrate to support LED assembly and electroplating. (a) Cross-section of the substrate. (b) A top view of the substrate.

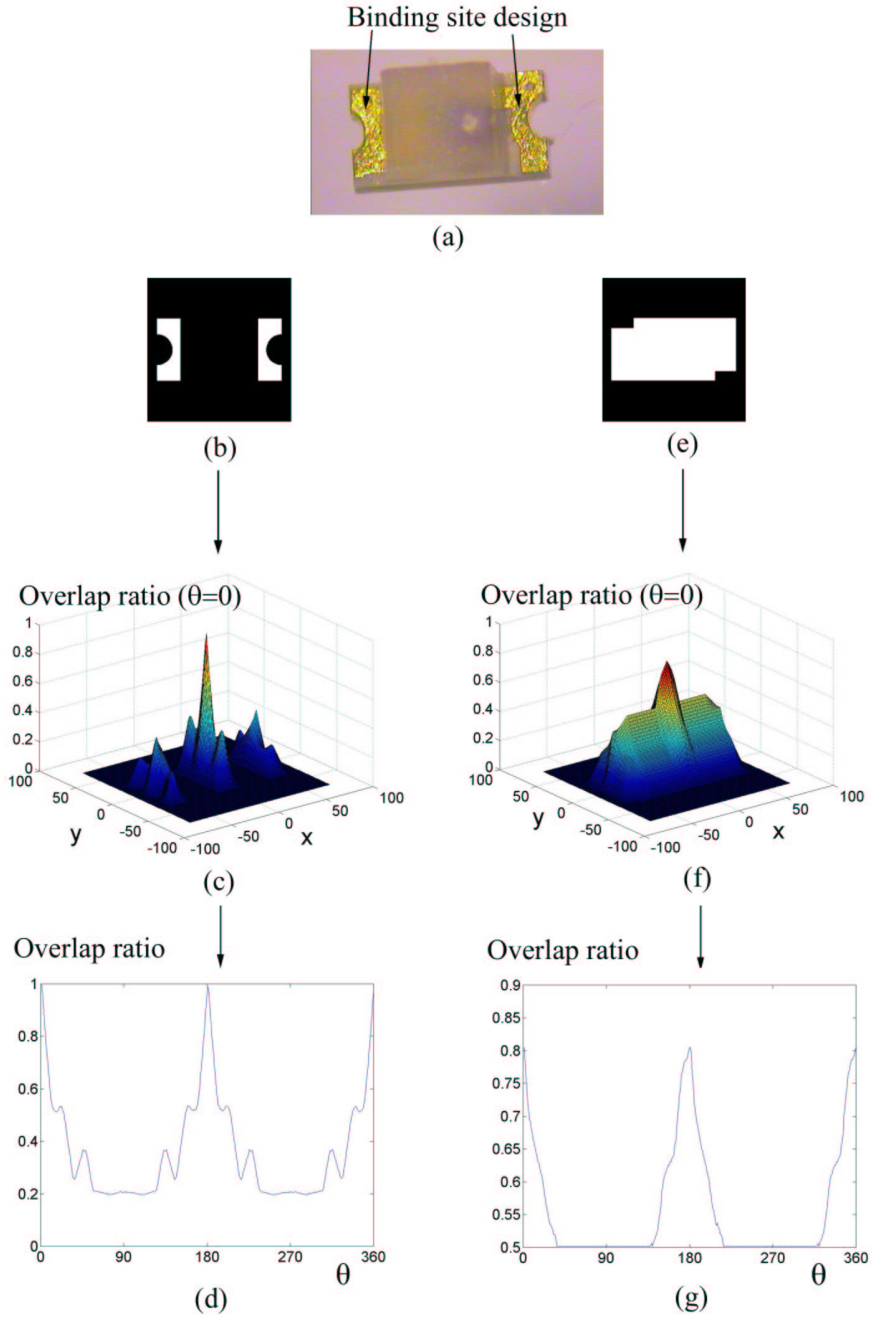

Figure 4: (a) A commercial LED with the given binding site design. (b) An intuitive design for the substrate binding site is the same as the binding site pattern of the LED. (c) Translation and (d) rotation simulations for the design in (b). (e) Another binding pattern design for LED assembly, with the openings on the top-left and bottom-right corners for placing the electroplating bases. (f) Translation and (g) rotation simulations for the design shown in (e).

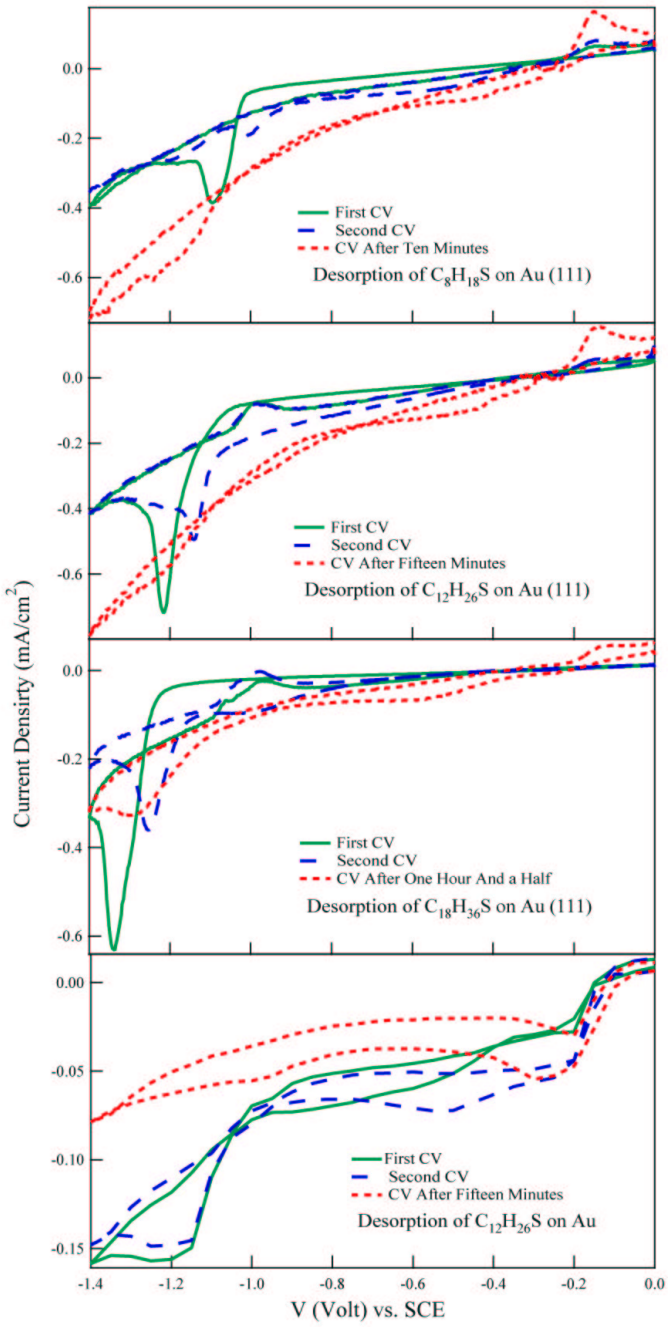

Figure 5: (a)-(c) CVs of SAM desorption from Au(111) on mica. (a) Octanethiol ($C_8H_{18}S$). (b) Dodecanethiolate ($C_{12}H_{26}S$). (c) Octadecanethiol ($C_{18}H_{38}S$). (d) CVs of dodecanethiolate ($C_{12}H_{26}S$) SAM desorption from polycrystalline Au on Si.

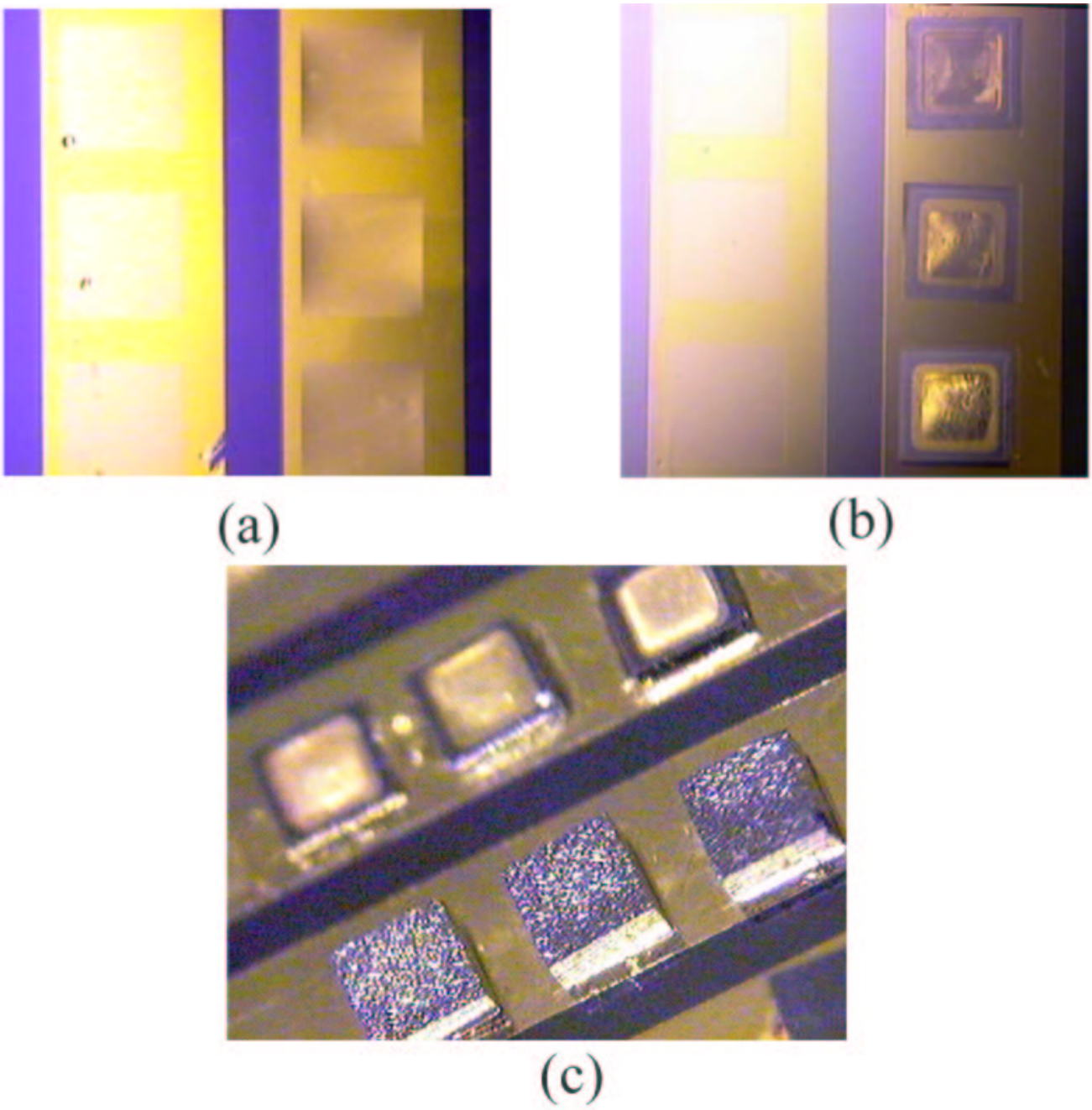

Figure 6: (a) A substrate with lubricant in water after selective SAM desorption. Reductive desorption has remove SAM from the Au squares on the left column. Lubricant wets the Au squares with SAM. (b) First batch of 1×1mm parts have been assembled and bonded only to Au patterns with lubricant on the right. (c) Side view of two-batch controlled micro assembly. Foreground: Second batch of 1×1mm assembled parts. Background: First batch of assembled parts.

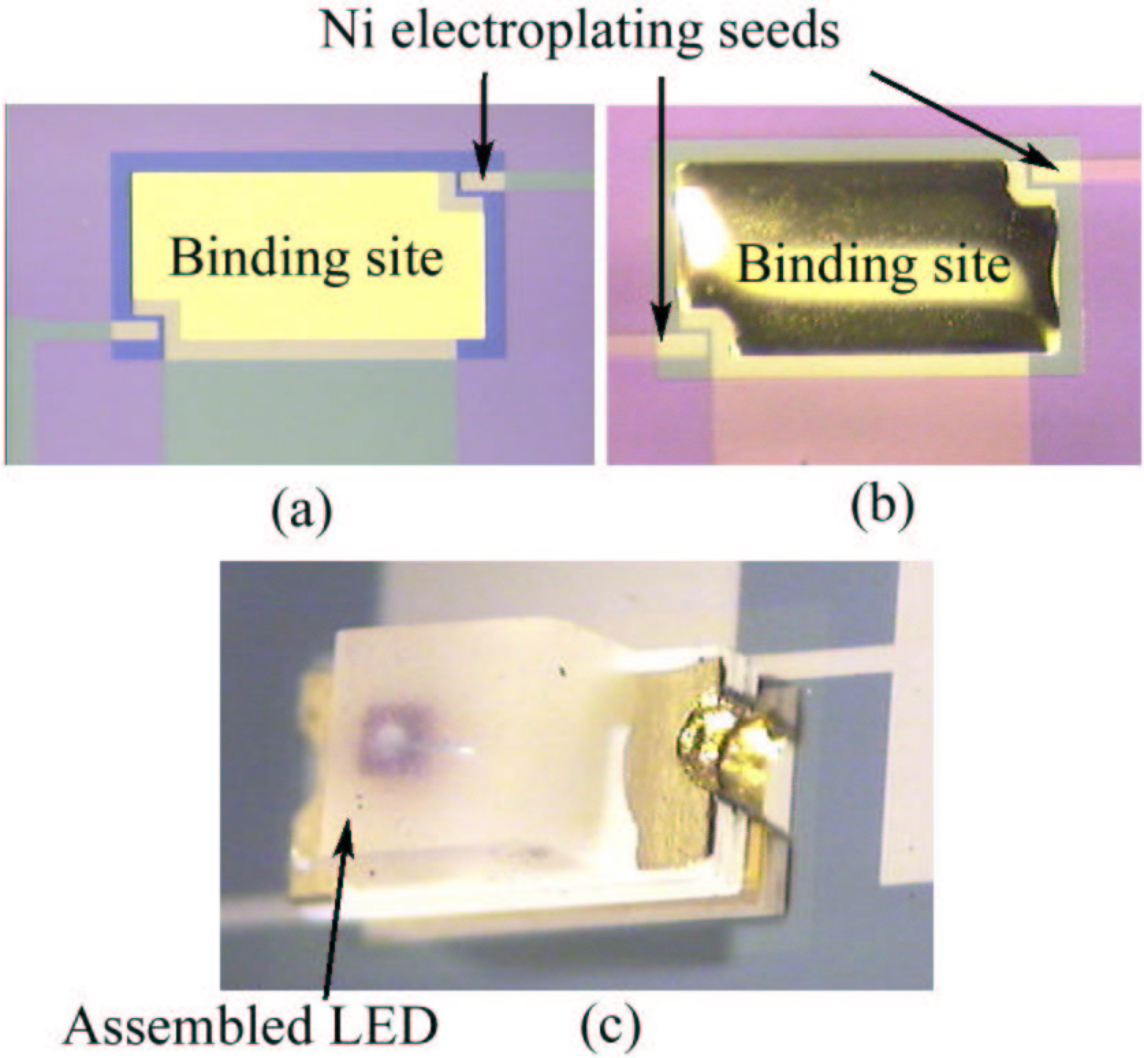

Figure 7: (a) A binding site designed for LED assembly. (b) A binding site with SAM after lubricant is applied. The exposed Ni electroplating bases remain clean. (c) An assembled LED on a binding site.

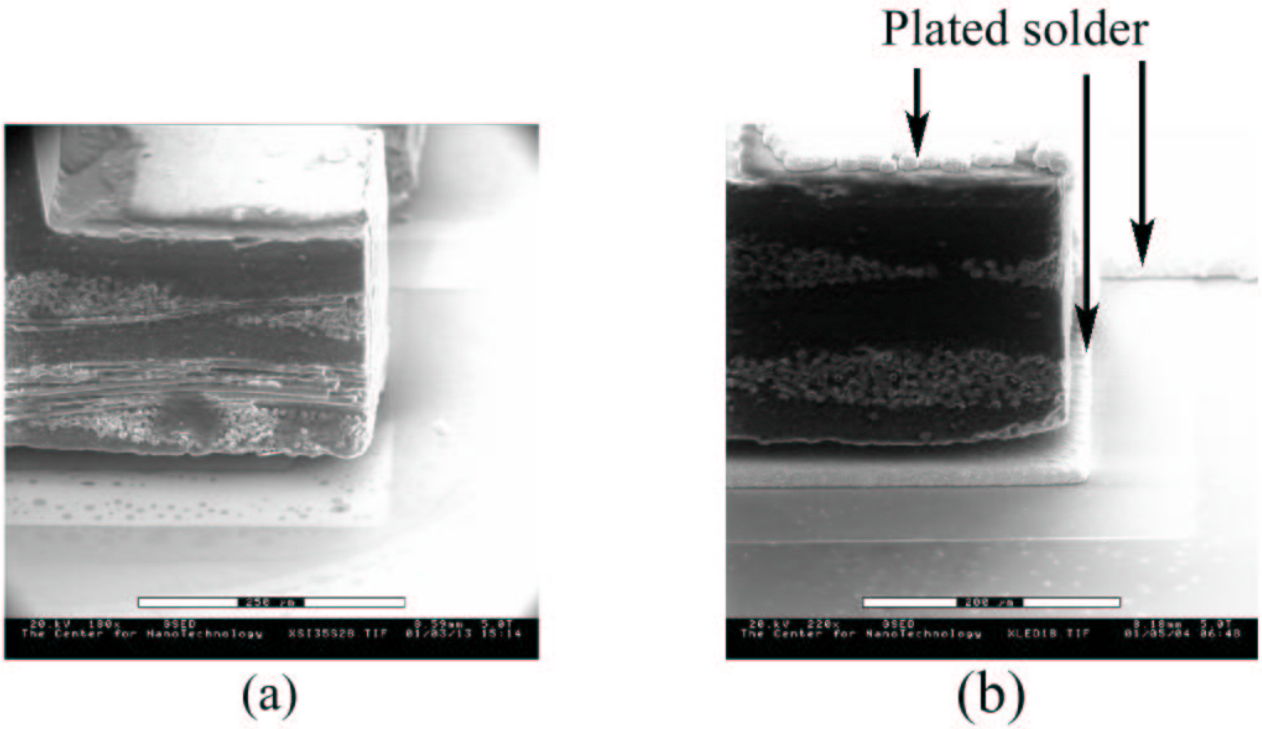

Figure 8: (a) An environmental scanning electron microscope (ESEM) image of an assembled LED. (b) An ESEM image of an assembled LED after electroplating.

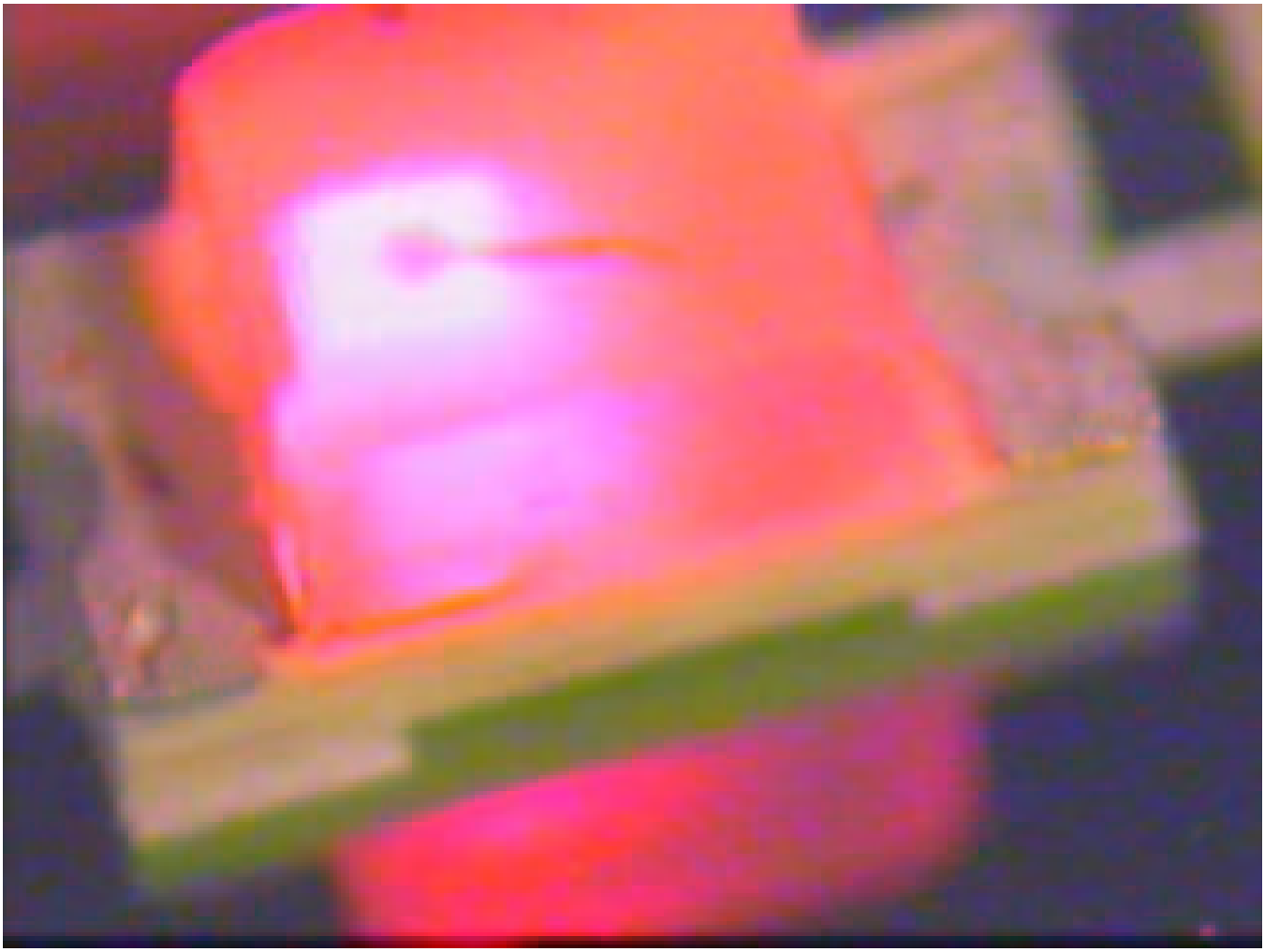

Figure 9: An LED on a substrate after electroplating. The LED is lightened by applying potential on the electrical contacts on the substrate.